1521-0111/12/8206-1042–1055$25.00
MOLECULAR PHARMACOLOGY
Vol. 82, No. 6
80267/3803723

Mol Pharmacol 82:1042–1055, 2012

Locating a Plausible Binding Site for an Open-Channel Blocker, GlyH-101, in the Pore of the Cystic Fibrosis Transmembrane Conductance Regulator[S]

Yohei Norimatsu, Anthony Ivetac, Christopher Alexander, Nicolette O'Donnell, Leah Frye, Mark S. P. Sansom, and David C. Dawson

Department of Physiology and Pharmacology, Oregon Health and Science University, Portland, Oregon (Y.N., C.A., N.O., D.C.D.); Department of Biochemistry, University of Oxford, Oxford, United Kingdom (A.I., M.S.P.S.); and Schrödinger Inc., Portland, Oregon (L.F.)

Received May 28, 2012; accepted August 24, 2012

ABSTRACT

High-throughput screening has led to the identification of small-molecule blockers of the cystic fibrosis transmembrane conductance regulator (CFTR) chloride channel, but the structural basis of blocker binding remains to be defined. We developed molecular models of the CFTR channel on the basis of homology to the bacterial transporter Sav1866, which could permit blocker binding to be analyzed in silico. The models accurately predicted the existence of a narrow region in the pore that is a likely candidate for the binding site of an open-channel pore blocker such as *N*-(2-naphthalenyl)-[(3,5-dibromo-2,4-dihydroxyphenyl)methylene]glycine hydrazide (GlyH-101), which is thought to act by entering the channel from the extracellular side. As a more-stringent test of predictions of the CFTR pore model, we applied induced-fit, virtual, ligand-docking techniques to identify potential binding sites for GlyH-101 within the CFTR pore. The highest-scoring docked position was near two pore-lining residues, Phe337 and Thr338, and the rates of reactions of anionic, thiol-directed reagents with cysteines substituted at these positions were slowed in the presence of the blocker, consistent with the predicted repulsive effect of the net negative charge on GlyH-101. When a bulky phenylalanine that forms part of the predicted binding pocket (Phe342) was replaced with alanine, the apparent affinity of the blocker was increased ~200-fold. A molecular mechanics-generalized Born/surface area analysis of GlyH-101 binding predicted that substitution of Phe342 with alanine would substantially increase blocker affinity, primarily because of decreased intramolecular strain within the blocker-protein complex. This study suggests that GlyH-101 blocks the CFTR channel by binding within the pore bottleneck.

Introduction

The cystic fibrosis transmembrane conductance regulator (CFTR) is a regulated anion channel (Riordan, 2008) and a key element in three devastating diseases, i.e., cystic fibrosis, secretory diarrhea, and polycystic kidney disease. Cystic fibrosis is a life-shortening, autosomal recessive, genetic disease characterized by decreased secretion of salt and water in the lungs and digestive system (Boucher, 2007). The disease is caused by mutations in CFTR that impair its trafficking and channel activity. Secretory diarrheas are a family of infectious diseases characterized by life-threatening intestinal hypersecretion of salt and water. The causative agents are enterotoxins, such as that produced by *Vibrio cholerae* (Sanchez and Holmgren, 2011); they increase cytosolic cAMP levels, which results in chronically active CFTR channels and unregulated salt and water loss. Polycystic kidney disease is a life-threatening genetic disease characterized by the presence of multiple cysts in the kidneys. The growth of cysts is

This work was supported by the National Institutes of Health National Institute of Diabetes and Digestive and Kidney Diseases [Grant DK45880]; the Cystic Fibrosis Foundation [Grant DAWSON08G0]; and the American Lung Association [Grant RT-7962-N]. The laboratory of M.S.P.S. was supported by the Wellcome Trust and the Biotechnology and Biological Sciences Research Council.

Article, publication date, and citation information can be found at http://molpharm.aspetjournals.org.

http://dx.doi.org/10.1124/mol.112.080267.

[S] The online version of this article (available at http://molpharm.aspetjournals.org) contains supplemental material.

ABBREVIATIONS: CFTR, cystic fibrosis transmembrane conductance regulator; 2-ME, 2-mercaptoethanol; DTT, dithiothreitol; MD, molecular dynamics; IFD, induced-fit docking; $EC_{50}(0)$, EC_{50} at 0 mV; MM-GB/SA, molecular mechanics-generalized Born/surface area; IBMX, 3-isobutyl-1-methylxanthine; $MTSET^+$, [2-(trimethylammonium)ethyl]methanethiosulfonate; $MTSES^-$, [2-sulfonatoethyl]methanethiosulfonate; NEM, *N*-ethyl maleimide; wt, wild-type; PDB, Protein Data Bank; TM, transmembrane segment; GlyH-101, *N*-(2-naphthalenyl)-[(3,5-dibromo-2,4-dihydroxyphenyl)methylene]glycine hydrazide; iOWH032, 3-(3,5-dibromo-4-hydroxyphenyl)-*N*-(4-phenoxybenzyl)-1,2,4-oxadiazole-5-carboxamide.

promoted by CFTR-mediated Cl^- secretion (Yang et al., 2008). These diseases, which occupy different parts of the spectrum of CFTR function, have motivated the search for small-molecule modulators of CFTR channels.

Compounds that block anion conduction through CFTR channels (Sheppard and Robinson, 1997; Cai et al., 1999; Muanprasat et al., 2004; Sheppard, 2004; Zhang et al., 2004a; Sonawane et al., 2006, 2007; de Hostos et al., 2011; Cui et al., 2012) may lead to treatments for secretory diarrhea and polycystic kidney disease. The CFTR-blocking small molecule 3-(3,5-dibromo-4-hydroxyphenyl)-*N*-(4-phenoxybenzyl)-1,2,4-oxadiazole-5-carboxamide (iOWH032), which currently is being studied in a clinical trial (de Hostos et al., 2011), is structurally related to the pore blocker *N*-(2-naphthalenyl)-[(3,5-dibromo-2,4-dihydroxyphenyl)methylene]glycine hydrazide (GlyH-101) (mol. wt., 493) (Fig. 1A). GlyH-101 carries a net negative charge (pK_a = 5.5) under physiological conditions (pH ~7.4) and is thought to block the CFTR by entering the channel from the extracellular side and binding to a site within the pore (Muanprasat et al., 2004; Sonawane et al., 2006, 2007). Although the mechanisms of action of pore blocking small molecules thought to act from the cytosolic side of the CFTR channel have been explored extensively in electrophysiological studies and amino acid substitution analyses (Sheppard and Robinson, 1997; Hwang and Sheppard, 1999; Zhou et al., 2002, 2010; Linsdell, 2005; Cui et al., 2012), the mechanism of action of GlyH-101 has been less well studied. We chose to investigate the binding of GlyH-101 because the open-channel blocker seemed likely to bind in a narrow part of the CFTR pore.

Molecular models, in combination with virtual ligand-docking algorithms, have been used successfully to identify novel small-molecule modulators of a variety of proteins through in silico screening of compound libraries (Villoutreix et al., 2009; Shoichet and Kobilka, 2012). These and related techniques also have been used to reveal the molecular basis for binding affinity (Dailey et al., 2009). We used a homology model of the CFTR, in conjunction with cysteine scanning mutagenesis, to identify a narrow "bottleneck" in the anion-conducting pore that seemed a likely site for the binding of GlyH-101 (Alexander et al., 2009; Norimatsu et al., 2012). The bottleneck was predicted to lie just cytoplasmic to the pore-lining residue Thr338 and to include the more-cytoplasmic pore-lining residue Ser341. This position was verified through comparisons of the reactivity of cysteines substituted in TMs 6 and 12 toward channel-permeant and channel-impermeant, thiol-directed probes. The larger, channel-impermeant probes reacted with a cysteine at position 338 but not with one at position 341, which indicates that residue 338 lies on the outward-facing rim of the bottleneck but residue 341 lies inside the narrow region. The goal of the studies described here was to use computational and experimental methods to identify and to analyze a plausible binding site for GlyH-101 in the CFTR pore.

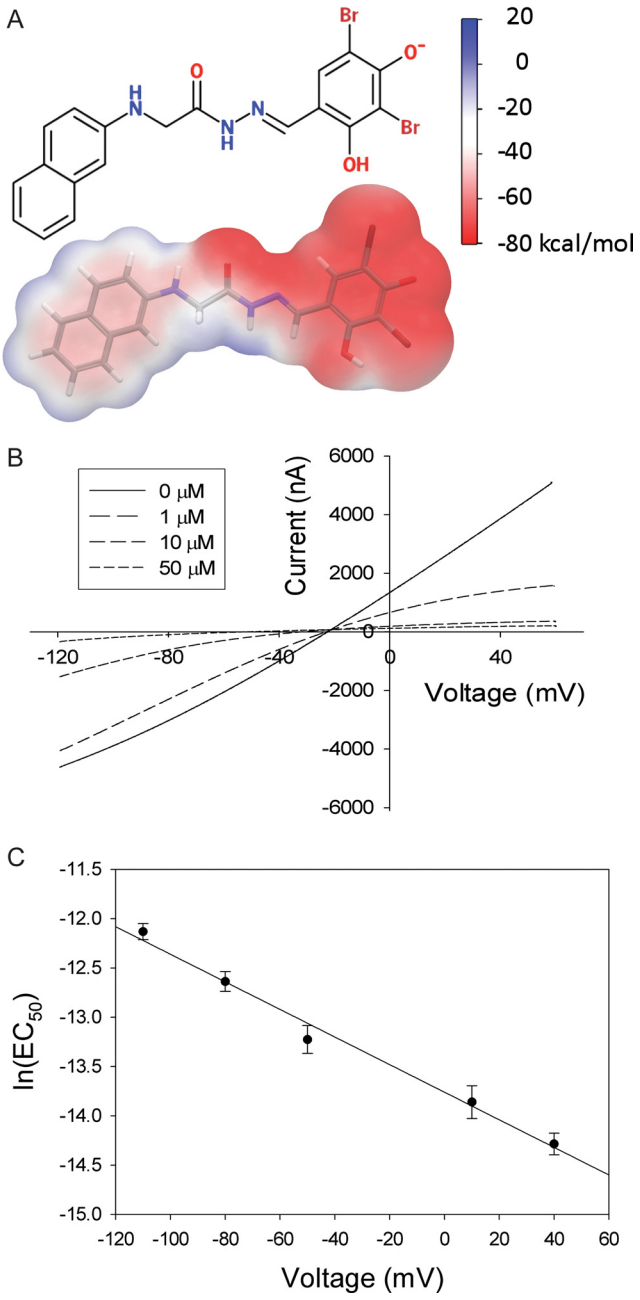

Fig. 1. A, structure of GlyH-101 in licorice representation with a transparent molecular surface. In the licorice representation, oxygen atoms are red, bromine brown, nitrogen blue, carbon gray, and hydrogen white. The molecular surface is colored according to the electrostatic potential energy. The scale bar shows the correspondence between the colors and electrostatic potential energy values. B, *I-V* curves in the absence and presence of 1, 10, and 50 μM GlyH-101. Wild-type CFTR channels were expressed in *Xenopus laevis* oocytes, and transmembrane currents were measured by using two-electrode, voltage-clamp methods. C, voltage dependence of the GlyH-101 EC_{50} for the wt CFTR, consistent with the Woodhull model (Woodhull, 1973; Tikhonov and Magazanik, 1998). See *Materials and Methods* for details. The EC_{50} at 0 mV was 1.1 ± 0.11 μM (n = 4), and the apparent electrical distance (from the outside) sensed by the blocker was 0.35 ± 0.013 (n = 4).

Materials and Methods

Mutagenesis and In Vitro Transcription. The methods used for mutagenesis and in vitro transcription were similar to those reported previously (Liu et al., 2001; Smith et al., 2001). A QuikChange site-directed mutagenesis kit (Agilent Technologies, Santa Clara, CA) was used to generate point mutations in a wt CFTR construct. Mutations were confirmed through direct DNA sequencing. The CFTR cRNAs for *Xenopus laevis* oocyte injection were synthesized by using a mMESSAGE mMACHINE T7 Ultra in vitro transcription kit (Invitrogen, Carlsbad, CA). After transcription, poly(A) tails were added to the transcripts by using *Escherichia coli* poly(A) polymerase, as described for the mMESSAGE mMACHINE T7 Ultra transcription kit.

Controlling for Spontaneous Reactions of Engineered Cysteines. All oocytes expressing cysteine-substituted CFTR constructs

were exposed to 2-mercaptoethanol (2-ME) or dithiothreitol (DTT) before exposure to any of the thiol-reactive probes used here. This protocol was based on extensive documentation of "spontaneous" changes in the chemical state of cysteine substituted at position 338 (Liu et al., 2006). We proposed that these spontaneous changes, which are not seen with either wt or cysteine-less CFTRs, reflect the coordination of trace amounts of copper (or some other, currently unidentified, metal) by the cysteine-substituted construct, which can be reversed with mobile metal ligands such as 2-ME, DTT, and CN^-.

Molecular Dynamics Simulation. Previously we built a homology model of CFTR that was based on the crystal structure of a bacterial homolog, Sav1866, and we performed a 30-ns molecular dynamics (MD) simulation with a dimyristoylphosphatidylcholine lipid bilayer by using the GROMOS96 force field (Norimatsu et al., 2012). Snapshots of the CFTR protein from the simulation were aligned through least-squares fitting using the C-α atoms. The conformational drift of the CFTR channel during the simulation, as indicated by the root mean square deviation of C-α atoms from the starting structure, suggested that equilibrium was reached by 4 ns (Norimatsu et al., 2012). On this basis, frames between 4 and 30 ns were used in this study.

Virtual Ligand Docking. The GlyH-101 molecule was constructed manually by using Maestro 9.1 (Schrödinger LLC., New York, NY) and was prepared for docking by using LigPrep 2.4 (Schrödinger). The ionization state was predicted with Epik 2.1 (Schrödinger) for the pH range of 6.4 to 8.4. The prediction was consistent with the pH-dependent ionic equilibria of GlyH-101 determined by Muanprasat et al. (2004), and the *p*-hydroxyl group on the benzene ring was deprotonated, carrying a single negative charge. The 4- to 30-ns snapshots of the CFTR were prepared for docking by using the protein preparation wizard (Schrödinger suite 2010; Epik 2.1; Schrödinger). GlyH-101 was virtually docked to each snapshot of the CFTR by using the induced-fit docking (IFD) protocol (Glide 5.6 and Prime 2.2; Schrödinger) described previously (Sherman et al., 2006). In the IFD protocol, the receptor protein is allowed to alter its conformation for better accommodation of the ligand. Each CFTR–GlyH-101 complex was assessed by using an empirical scoring function called the GlideScore (Friesner et al., 2006). The complex with the best GlideScore was chosen for the study. This approach is similar to that used by Rao et al. (2008), who investigated the performance of different conformational ensembles of p38 mitogen-activated protein kinase for in silico screening of diverse compounds and found that GlideScores represented an appropriate metric for the prediction of binding modes. The structure of the F342A CFTR was generated with Maestro 9.1 by replacing Phe342 of the wt CFTR in the predicted complex with alanine. GlyH-101 was docked to the structure of the F342A CFTR by using the IFD protocol, and the structure of the resulting complex was used for MM-GB/SA analysis (see *Calculation of Binding Free Energy* for more details).

Preparation and Microinjection of Oocytes. The preparation and microinjection of *X. laevis* oocytes were performed by using methods described previously (Liu et al., 2006). The follicular membranes were removed through mechanical agitation (1–2 h) in Ca^{2+}-free solution containing 82.5 mM NaCl, 2 mM KCl, 1 mM $MgCl_2$, 5 mM HEPES hemisodium salt, pH 7.5, and 0.2 Wünsch units/ml Liberase Blendzyme 3 (Roche Molecular Biochemicals, Indianapolis, IN). Defolliculated oocytes were washed and maintained in modified Barth's solution containing 88 mM NaCl, 1 mM KCl, 0.82 mM $MgSO_4$, 0.33 mM $Ca(NO_3)_2$, 0.41 mM $CaCl_2$, 2.4 mM $NaHCO_3$, 10 mM HEPES hemisodium salt, and 250 mg/liter amikacin, pH 7.5. CFTR cRNA and cRNA encoding the human β_2-adrenergic receptor were injected into stage V to VI oocytes. CFTR cRNA was diluted to yield 50 to 200 μS of stimulated conductance, i.e., ~0.2 ng/oocyte in a 50-nl volume for most constructs.

Whole-Cell Recordings. The whole-cell recording methods used in the current study were similar to those described by Mansoura et al. (1998). Individual oocytes were placed in the recording chamber and continuously superfused with frog Ringer's solution. The Ringer's solution contained 98 mM NaCl, 2 mM KCl, 1 mM $MgCl_2$, 1.8 mM $CaCl_2$, and 5 mM HEPES hemisodium salt, pH 7.4. A TEVC-200 amplifier (Dagan, Minneapolis, MN) and the pClamp 8 data acquisition program (Molecular Devices, Sunnyvale, CA) were used for data acquisition. Oocytes were maintained in the open-circuit condition, and the membrane potential was periodically ramped from −120 to +60 mV over 1.8 s for construction of the whole-cell *I-V* plots. For some experiments, a step protocol was used for current recordings. At the beginning of each trace, the voltage was held at 0 mV for 0.5 s; it was then stepped to −110, −80, −50, −20, +10, or +40 mV for 2 to 5 s. After this step, the voltage was held at either 0 or +40 mV for 5 to 10 s, to reach a steady current. Blockade by GlyH-101 was determined with concentrations ranging from 1 nM to 100 μM. The EC_{50} was determined for each voltage through fitting of a dose-response curve. The voltage dependence of the EC_{50} was analyzed by using a modified version of the Woodhull model (Woodhull, 1973; Tikhonov and Magazanik, 1998), $EC_{50}(V) = EC_{50}(0)\exp(z\delta VF/RT)$, where $EC_{50}(0)$ is the EC_{50} at 0 mV, z is the valence of the blocker, δ is the fractional electrical distance of the binding site from the extracellular bulk solution, V is the transmembrane voltage, and F, R, and T have their usual meanings.

Calculation of Binding Free Energy. The MM-GB/SA method described by Guimarães and Cardozo (2008) was used to compute an estimate of the free energy of binding, ΔG_{bind}, as $\Delta G_{bind} = \Delta E_{lig} + \Delta G_{solv} - T\Delta S_{conf} + E_{vdw} + E_{es} + \Delta E_{PTN}$, where ΔE_{lig} and ΔE_{PTN} are changes (upon ligand binding) in the intramolecular strains of the ligand and protein, respectively, ΔG_{solv} is the total desolvation penalty for the ligand and protein, $T\Delta S_{conf}$ is the ligand conformational penalty, and E_{vdw} and E_{es} are the van der Waals and electrostatic energies, respectively. This method was used successfully for rank-ordering of compounds, in terms of binding affinities, for proteins such as cyclin-dependent kinase 2, factor Xa, thrombin, and HIV-1 reverse transcriptase (Guimarães and Cardozo, 2008). Similar MM-GB/SA techniques were used to investigate the effects of protein mutations on ligand binding affinity (Carra et al., 2012). In the current study, the Embrace function of MacroModel 9.8 (Schrödinger) was used for the MM-GB/SA calculations. The CFTR–GlyH-101 complex, CFTR alone, and GlyH-101 alone were energy-minimized by using a conjugate gradient minimization scheme (Polak-Ribière conjugate gradient). The free energy of binding was calculated as the energy difference between the CFTR–GlyH-101 complex in water and the CFTR alone plus GlyH-101 alone in water. The calculation was also performed with the channel inserted in a bilayer containing explicit dimyristoylphosphatidylcholine lipid molecules. The coordinates of membrane lipid molecules were derived from the MD simulation described by Norimatsu et al. (2012). The Optimized Potential for Liquid Simulations 2005 force-field was used to calculate intramolecular and intermolecular energies, and a generalized Born/surface area model was used to calculate solvation energies. In the energy minimization, no constraints were applied to residues within 10 Å of GlyH-101. A second shell of 5 Å around the first shell was defined, and harmonic restraints with a force constant of 200 kcal/mol per $Å^2$ were applied to residues within that shell. A third shell of 5 Å around the second shell was defined, and residues within that shell were held fixed. The remaining residues were ignored. The membrane lipid molecules also were held fixed during the energy minimization. To avoid steric clashes between side chains of the CFTR channel and frozen lipid molecules, lipid molecules within 3 Å of the channel were removed. The number of lipid molecules included in the system was limited to 86 (10,148 atoms), to improve computing efficiency.

Reagents. The experiments presented here were conducted by using 10 μM isoproterenol and 1 mM IBMX (Sigma-Aldrich, St. Louis, MO) as the stimulating cocktail. Methanethiosulfonate reagents ($MTSET^+$ and $MTSES^-$) were purchased from Toronto Research Chemicals (North York, ON, Canada). 2-ME, DTT, *N*-ethlymaleimide (NEM), and potassium dicyanoaurate(I) ($K[Au(CN)_2]$) were obtained from Sigma-Aldrich. KCN was obtained from Thermo Fisher Scientific (Waltham, MA).

Results

Ensemble IFD of GlyH-101 Predicts a Binding Mode near Thr338. Figure 1A shows the structure of GlyH-101 and the electrostatic potential at its molecular surface predicted with Jaguar 7.7 (Schrödinger). The molecule is composed of a hydrophobic naphthalene tail and a negatively charged dibromodihydroxyphenyl head. According to atomic partial charges assigned with Antechamber (http://ambermd.org) (Wang et al., 2006), more than 80% of the net negative charge of GlyH-101 resides within the dibromodihydroxyphenyl group. The representative *I-V* plots shown in Fig. 1B confirm the report by Muanprasat et al. (2004) that blockade of the wt CFTR by GlyH-101 is highly voltage-dependent, in the manner predicted for a negatively charged molecule that enters the pore from the outside and binds to a site within the pore. As illustrated, the blockade by 1 μM GlyH-101 was relieved when the transmembrane potential was negative. Figure 1C contains the results of a Woodhull analysis (Woodhull, 1973; Tikhonov and Magazanik, 1998) of the voltage-dependent blockade of the wt CFTR by GlyH-101, which yielded a value of 0.35 ± 0.013 (n = 4) for the fraction of the electric potential sensed by the blocker as it enters the channel from the outside and a value of 1.1 ± 0.11 μM (n = 4) for $EC_{50}(0)$. This behavior is consistent with a "cork-in-the-bottle" type of open-channel block, in which the bound blocker is expected to lodge in a narrow portion of the pore and obstruct anion flow on the basis of its negative charge and bulk. An IFD protocol (Sherman et al., 2006) that permits modeling of protein conformational changes around the ligand (see *Materials and Methods* for details) was used to dock GlyH-101 in the predicted bottleneck region of the CFTR pore. The IFD protocol was applied to 27 MD snapshots (4–30 ns) derived from a previously described 30-ns MD simulation (Norimatsu et al., 2012) of the CFTR in a lipid membrane with explicit water molecules (the structure of the 9-ns snapshot of the CFTR is presented in Supplemental PDB File 1). The best GlideScore (−9.7 kcal/mol) was obtained for a binding mode in the 9-ns snapshot illustrated in Fig. 2 (the structure of the predicted complex is presented in Supplemental PDB File 2).

In the predicted binding mode (Fig. 2), the hydrophobic naphthalene tail sits in a hydrophobic pocket lined by the bulky side chain of Phe342, whereas the negatively charged head protrudes into the outer vestibule of the pore in the vicinity of two residues, Phe337 and Thr338. When either Phe337 or Thr338 was replaced with cysteine, the EC_{50} for GlyH-101 blockade at 0 mV was only modestly increased (Table 1).[1] Increasing the bulk of either cysteine side chain through alkylation with iodoacetamide further increased the $EC_{50}(0)$ ~6-fold for position 338 but only 1.3-fold for position 337. Views of the predicted blocker-CFTR complex shown in Supplemental Fig. 1 indicate that addition of the acetamide moiety to a cysteine at position 338 would produce a steric clash with the proposed binding conformation of GlyH-101, whereas the same addition at position 337 would not. Previous studies documented the important role of the positive charge on Lys95 in the binding of blockers (such as glibenclamide) that enter the pore from the cytosolic side (Linsdell, 2005; Zhou et al., 2010). Replacing Lys95 with cysteine had little impact on the $EC_{50}(0)$ for GlyH-101 (Table 1), however, consistent with the notion that the GlyH-101 binding site does not overlap with those of the cytoplasmic blockers.

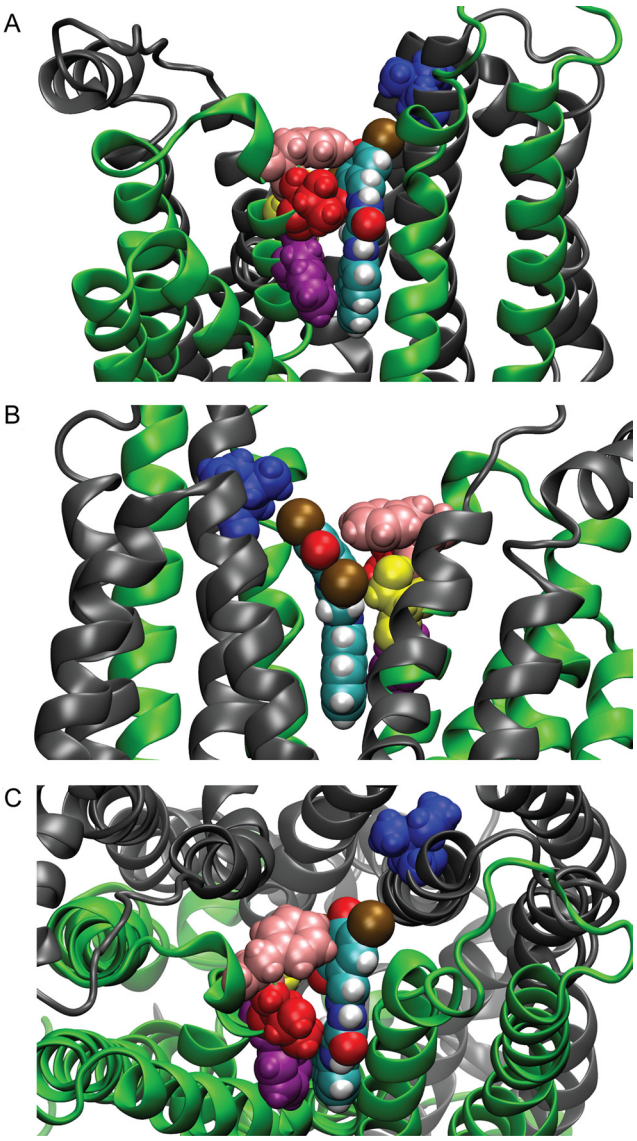

Fig. 2. Predicted binding mode for GlyH-101. A, view from the side of transmembrane domain 1 (green). B, view from the side of transmembrane domain 2 (gray). C, top view from the extracellular side. Phe337 is displayed in pink, Thr338 in red, Ser341 in yellow, Phe342 in purple, and Ile1131 in blue. Our model of the CFTR shows that both Phe337 and Thr338 lie close to the negatively charged GlyH-101 when it is bound in the pore. Phe337, Thr338, and Ile1131 were each mutated to cysteine in silico (Maestro; Schrödinger), and the distances between the sulfur atom of the thiol group and each of the six carbon atoms in the benzene ring of GlyH-101 were measured. The average distances to the benzene ring from the sulfur atom were 5.9 Å for position 337 and 7.3 Å for position 338. Both values are less than the Debye length (9.2 Å) in frog Ringer's solution. The distance from position 1131 was 11.5 Å. The position of Ser341 indicates that it might be protected from electrically neutral reagents through steric hindrance provided by bound GlyH-101.

[1] The modest impact of the cysteine substitution at position 338 on the apparent affinity of GlyH-101 was unexpected, in view of our previous demonstration of a pH-dependent, partial, negative charge on a cysteine at this position (Liu et al., 2004). Under the conditions of the present experiments (pH 7.4) and with the measured pK_a of 7.3, the cysteine partial charge would be predicted to be ~0.5. The net negative charge of bound GlyH-101, however, is expected to promote protonation of the cysteine at position 338, which would effectively shift the pK_a to a more-basic value and thus substantially reduce the net negative charge on the cysteine, as reported previously for a stromelysin inhibitor (Parker et al., 1999).

TABLE 1
EC_{50} at 0 mV (mean ± S.E.M.) for GlyH-101 for wt and mutant CFTRs, with and without modification with iodoacetamide

CFTR	EC_{50} at 0 mV
	μM
wt	1.1 ± 0.11 (n = 4)
K95C	1.4 ± 0.35 (n = 4)
F337C	1.8 ± 0.06 (n = 3)
F337C + iodoacetamide	2.4 ± 0.29 (n = 3)
T338C	3.7 ± 0.27 (n = 3)
T338C + iodoacetamide	24 ± 2.6 (n = 3)

The presence of the negatively charged head of GlyH-101 near positions 337 and 338 is expected to alter the reactions of anionic, thiol-directed reagents with cysteines substituted at those positions. Because GlyH-101 is an open-channel blocker, however, protection of an engineered cysteine by GlyH-101 is expected only if the engineered cysteine reacts with thiol-directed probes primarily in the open state of the channel. Therefore, we began by investigating the state dependence of reactions between engineered cysteines and thiol-directed probes.

Reactions of Engineered Cysteines at Positions 334, 337, and 338 with Externally Applied, Thiol-Directed Reagents Are State-Dependent. Figure 3 illustrates the protocol used to investigate the state dependence of the reactivity of cysteines substituted at positions 334, 337, and 338. In this example, externally applied $[Au(CN)_2]^-$ was reacted with the F337C CFTR. We showed previously that the ligand-exchange reaction of $[Au(CN)_2]^-$ with cysteines at positions 337 and 338 reduces channel conductance by depositing the negatively charged $[AuCN]^-$ moiety on the thiol (Serrano et al., 2006; Alexander et al., 2009). Therefore, the time course of the ligand-exchange reaction can be monitored by recording the decrease in membrane conductance after the application of $[Au(CN)_2]^-$. The reactions do not reverse spontaneously but can be reversed through exposure of the channel to CN^- (a high-affinity metal ligand), in the form of KCN (Serrano et al., 2006; Alexander et al., 2009). We compared the $[Au(CN)_2]^-$ reaction rate observed when oocytes were exposed to the reagent before activation, when channels were mostly closed, with that seen when oocytes were exposed to $[Au(CN)_2]^-$ after activation of CFTR channels. In the case of preactivation exposure, the extent of the reaction was judged by determining the conductance recovered with exposure to KCN after subsequent channel activation (Fig. 3B). Application of the high-affinity metal ligand revealed any ligand-exchange reaction that occurred before channel activation, when the channels were primarily in the closed state.

Figure 3, C and D, contains the time courses for the reactions of $[Au(CN)_2]^-$ with the F337C and T338C CFTRs before

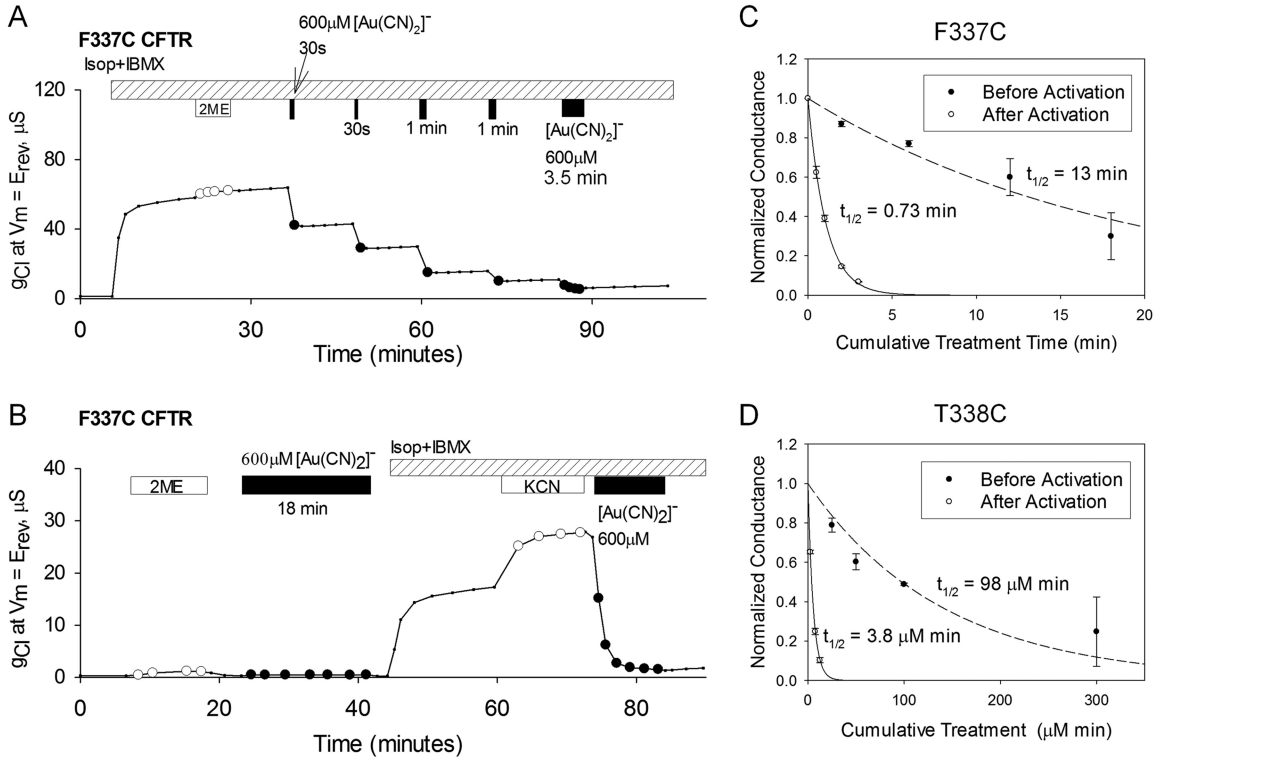

Fig. 3. State-dependent reactivity of the F337C CFTR with $[Au(CN)_2]^-$. A, exposure of an oocyte to 30-s and 1-min pulses of 600 μM $[Au(CN)_2]^-$ resulted in reductions of conductance. Covalent labeling of the F337C CFTR was almost complete after a cumulative exposure time of 2 min. Isop, isoproterenol. B, before activation of the F337C CFTR with isoproterenol and IBMX, 600 μM $[Au(CN)_2]^-$ was applied to the oocyte for 18 min. The conductance was partially reduced, as demonstrated by the additional increase in conductance with the application of 1 mM KCN. The subsequent application of $[Au(CN)_2]^-$ almost completely abolished F337C CFTR conductance. C and D, time courses of the decreases in normalized conductance as a result of F337C (C) and T338C (D) modifications with $[Au(CN)_2]^-$. Data points represent mean ± S.E.M. (n = 3). For the F337C CFTR, the abscissa represents cumulative $[Au(CN)_2]^-$ exposure time. For the T338C CFTR, the abscissa represents cumulative $[Au(CN)_2]^-$ exposure (exposure time × $[Au(CN)_2]^-$ concentration used). The reaction rate for the F337C CFTR before activation of the channels was ~20 times slower than the rate after activation. The rate for the T338C CFTR was almost 30 times slower before activation. The lines represent the best fits of single-exponential functions to the conductance data. The half-life of each single-exponential fit is shown. The second-order reaction rate constants for the F337C CFTR before and after activation were 1.5 and 26 M^{-1} s^{-1}, respectively. The second-order reaction rate constants for the T338C CFTR before and after activation were 1.2 × 10^2 and 3.0 × 10^3 M^{-1} s^{-1}, respectively.

and after activation. In the case of the T338C CFTR, different concentrations of $[Au(CN)_2]^-$ were used to construct the time course (50 μM for the preactivation rate and 5 μM for the postactivation rate), to compensate for the slower reaction rate in the preactivation condition. The abscissa indicates cumulative exposure, that is, the product of probe concentration and time. The reaction of $[Au(CN)_2]^-$ with a cysteine at position 338 was shown previously to follow second-order kinetics (Serrano et al., 2006), so different concentrations can be used to estimate reaction rate constants. The reactions of cysteines at both locations were favored in the active state, by ~20-fold for position 337 and by nearly 30-fold for position 338. We demonstrated previously that activation of CFTR channels in *X. laevis* oocytes is attributable entirely to the opening of channels that reside on the surface (Liu et al., 2001); channels are not recruited to the cell surface during the cAMP-dependent activation process. The results depicted in Fig. 3 indicate that the accessibility of cysteines at positions 337 and 338 to an externally applied, thiol-directed reagent is favored in the activated state of the channel.

With respect to the state-dependent reactivity of engineered cysteines toward externally applied reagents, it was suggested that it might be possible to distinguish between the closed state of the channel before phosphorylation (the preactivation state in the current study) and the closed state that is visited transiently, after phosphorylation, during ATP-dependent channel gating (Fatehi and Linsdell, 2008). As a test of this notion, we compared the modification rates before and after activation for a cysteine substituted at position 334. Zhang et al. (2005), in an elegant series of experiments, showed in single-channel recordings that modification by externally applied $MTSET^+$ of a cysteine substituted at position 334 occurred exclusively when the actively gating channel was in the closed state. Figure 4 shows the time courses for the reactions of $[Au(CN)_2]^-$ and $MTSET^+$ with R334C CFTR channels. The positive charge deposited by $MTSET^+$ at this location increased CFTR conductance, as reported previously (Smith et al., 2001; Zhang et al., 2005). Reaction rates for both reagents were 2- to 3-fold greater when oocytes were exposed to reagent before CFTR activation. The consistency of our findings and those of Zhang et al. (2005) suggests that, with respect to the reactivity of a cysteine substituted at position 334, the preactivation and postactivation closed states are operationally equivalent. These states also are expected to be similar in that the nucleotide-binding domains are partially dissociated in both conditions (Mense et al., 2006; Csanády et al., 2010). Beck et al. (2008) studied R334C CFTR channels expressed in *X. laevis* oocytes by using a protocol similar to that used here, but they failed to detect increased reactivity toward externally applied 2-aminoethylmethanethiosulfonate in the activated state. The latter probe, however, is well known for its capacity to exist in an uncharged, membrane-permeant form (Holmgren et al., 1996; Smith et al., 2001), which may explain the lack of state dependence observed for 2-aminoethylmethanethiosulfonate.

If we assume, on the basis of the report by Zhang et al. (2005), that the modification rates for $MTSET^+$ and $[Au(CN)_2]^-$ are approximately 0 for open channels, then it is possible to estimate the open probability indicated by the 2- to 3-fold difference in reaction rates observed in our experiments. As suggested by del Camino et al. (2000), the thiol modification rate constant, before or after activation, can be expressed as a weighted average of the modification rates for open and closed channels, $\kappa_{ob} = f_c \times \kappa_c + (1 - f_c) \times \kappa_o$, where κ_{ob} is the observed reaction rate constant, f_c is the closed probability of the channels, and κ_c and κ_o are the reaction rate constants for the closed and open channels, respectively. Inserting $\kappa_o = 0$ into eq. 2 yields a value for the postactivation closed probability, f_c, of 0.3 to 0.5 (open probability of ~0.5–0.7) (see Appendix for details), values qualitatively consistent with the results of previous studies (Fischer and Machen, 1994; Cai et al., 2003; Bompadre et al., 2005).

Engineered Cysteines at Positions 337, 338, and 341 Are Protected from Thiol-Directed Reagents by GlyH-101. Figure 5, A and B, illustrates the protocol, similar to that used by del Camino et al. (2000), that was used to investigate the possible protection of cysteines at positions 337, 338, and 341 by GlyH-101. Figure 5A presents a representative time course showing the cumulative effects of 30-s

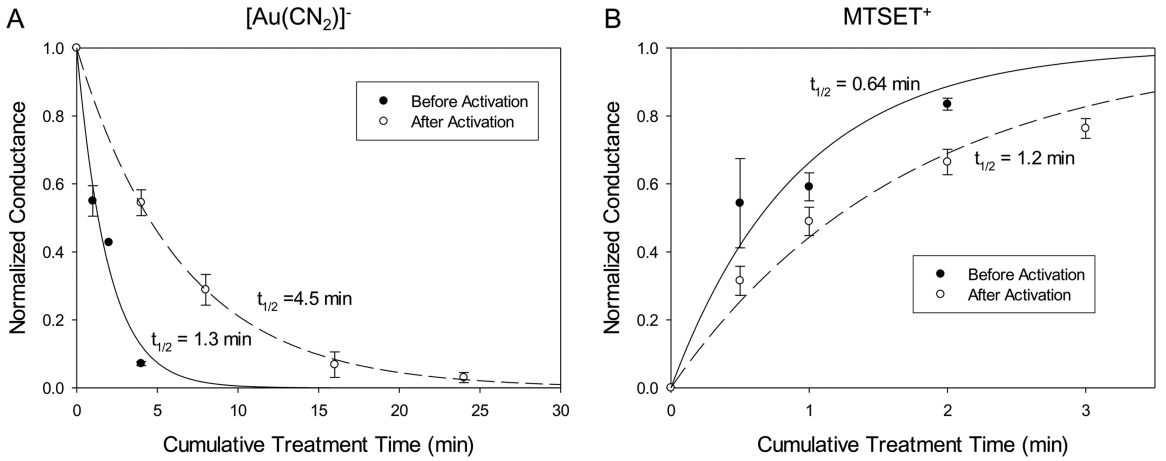

Fig. 4. Time courses of reactions of R334C (an engineered cysteine at position 334) with 10 μM $[Au(CN)_2]^-$ (A) or 250 nM $MTSET^+$ (B). Data points represent mean ± S.E.M. ($n = 3$). The abscissa represents the cumulative reagent exposure time. The lines represent the best fits of single-exponential functions to the conductance data. The half-life of each single-exponential fit is shown. For both $[Au(CN)_2]^-$ and $MTSET^+$, the reaction rate for the R334C CFTR before activation of the channels was faster than the rate after activation. The second-order reaction rate constants for $[Au(CN)_2]^-$ before and after activation were 8.9×10^2 and 2.6×10^2 M^{-1} s^{-1}, respectively. The second-order reaction rate constants for $MTSET^+$ before and after activation were 7.2×10^4 and 3.9×10^4 M^{-1} s^{-1}, respectively.

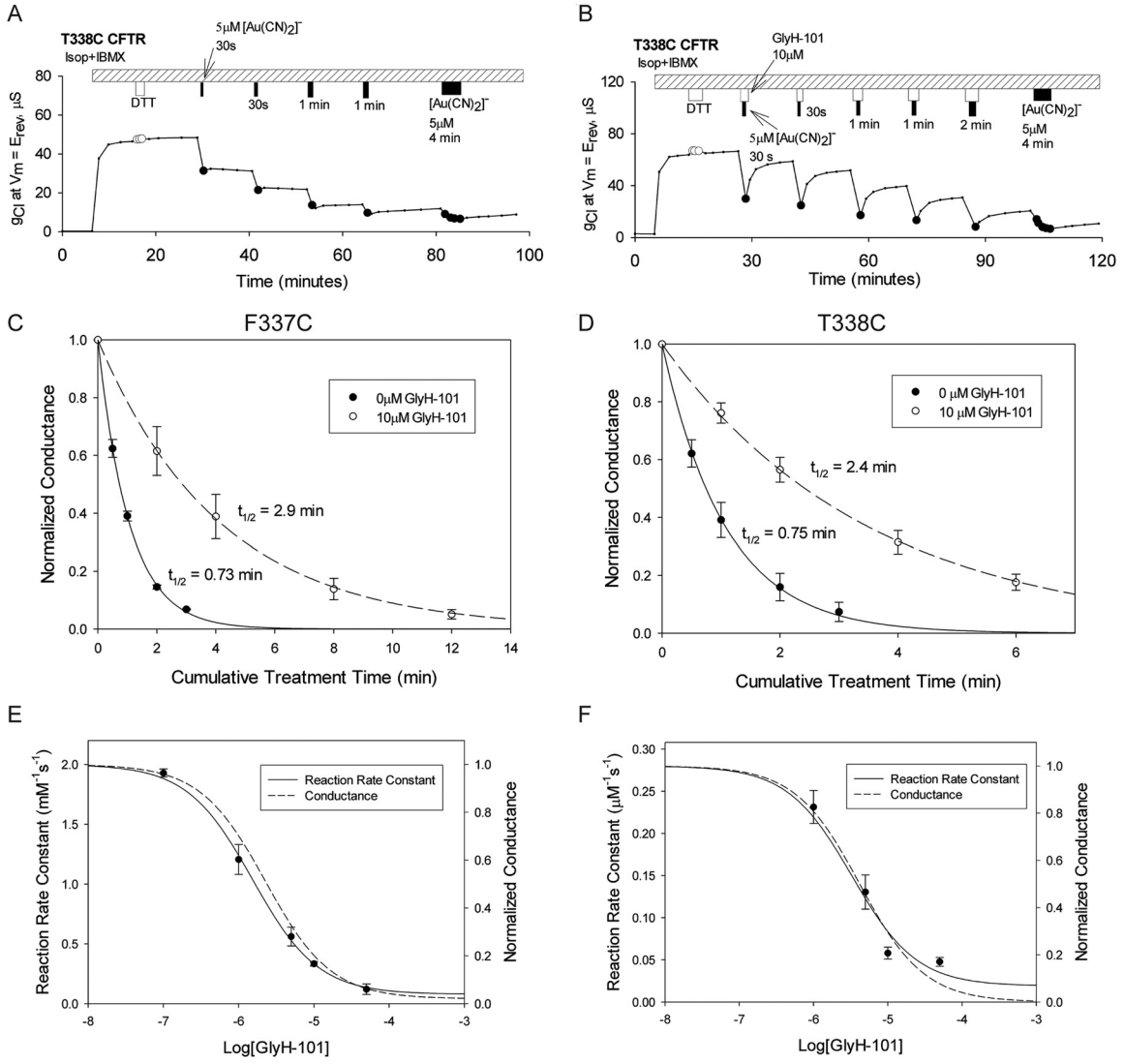

Fig. 5. GlyH-101 protection of T338C (an engineered cysteine at position 338) from modification by $[Au(CN)_2]^-$. A, exposure of an oocyte to 30-s and 1-min pulses of 5 μM $[Au(CN)_2]^-$ resulted in reductions of conductance. Covalent labeling of the T338C CFTR was almost complete after a cumulative exposure time of 2 min. Isop, isoproterenol. B, the oocyte was exposed to 5 μM $[Au(CN)_2]^-$ in the presence of 10 μM GlyH-101. The blockade attributable to covalent labeling was less than 50% after a cumulative exposure time of 2 min. The application of GlyH-101 was started 30 s before the application of $[Au(CN)_2]^-$, to ensure maximal blockade of the channels during the $[Au(CN)_2]^-$ reaction. The GlyH-101 application was continued 30 s after the end of the $[Au(CN)_2]^-$ application. C and D, F337C (C) and T338C (D) CFTR channels were protected by 10 μM GlyH-101 from reactions with $[Au(CN)_2]^-$. Data points represent mean ± S.E.M. (n = 3). The F337C CFTR was reacted with 600 μM $[Au(CN)_2]^-$ and the T338C CFTR was reacted with 5 μM $[Au(CN)_2]^-$ in the presence and absence of 10 μM GlyH-101. The lines represent the best fits of single-exponential functions to the normalized conductance data. The half-life of each single-exponential fit is shown. E and F, the rates of reaction of $[Au(CN)_2]^-$ with F337C (E) and T338C (F) CFTRs decreased as the concentration of GlyH-101 was increased. Data points represent mean ± S.E.M. (n = 3). Solid lines, best fits of sigmoidal dose-response curves to the reaction rate data. Dashed lines, dose-response curves for GlyH-101 blockade of the cysteine-substituted constructs observed in this study. The reaction rate constant observed in the absence of GlyH-101 was used as the maximal value of the sigmoidal curve. The EC_{50} and the minimal rate constant for the F337C CFTR were 1.6 μM and 0.08 $mM^{-1}\ s^{-1}$, respectively; values for the T338C CFTR were 3.3 μM and 0.02 $\mu M^{-1}\ s^{-1}$. The $EC_{50}(0)$ values for GlyH-101 blockade for the F337C and T338C CFTRs were 1.8 ± 0.063 (n = 3) and 3.7 ± 0.27 μM (n = 3), respectively.

and 1-min applications of 5 μM $[Au(CN)_2]^-$ to an oocyte expressing T338C CFTR. A similar procedure, in which $[Au(CN)_2]^-$ was applied during brief exposures of the oocyte to GlyH-101 and the extent of the reaction was estimated from the conductance recovered after washout of the blocker, is illustrated in Fig. 5B. Inspection of the response to the first, 30-s exposure revealed that the extent of modification of T338C CFTR conductance by $[Au(CN)_2]^-$ was markedly reduced when the reagent was applied in the presence of the blocker. Figure 5, C and D, summarizes the inhibition of the F337C and T338C CFTRs by $[Au(CN)_2]^-$ in the presence and absence of GlyH-101. In both cases, the time course of cysteine modification was slowed in the presence of the reversible blocker, as would be expected if the negative charge on the bound GlyH-101 repelled the negatively charged pseudohalide probe, thereby partially protecting the engineered cysteine from the ligand-exchange reaction with $[Au(CN)_2]^-$.

Because GlyH-101 is a reversible blocker, the extent of protection should exhibit a dose-response relationship similar to that of channel blockade. In Fig. 5, E and F, the measured second-order rate constants for covalent modification of the F337C and T338C CFTRs are plotted versus the

GlyH-101 concentration. In each case, the dose-response data could be fit with a Hill coefficient of 1 and the curves were virtually identical to those describing the dose dependence of blockade of the cysteine-substituted channels by GlyH-101, which suggests that, whenever the channel is blocked by GlyH-101, the engineered cysteine is protected. The protection of engineered cysteines at positions 337 and 338 from reaction with $[Au(CN)_2]^-$ is consistent with the model suggested in Fig. 2, in which GlyH-101 binds to a site within the anion conduction pathway that places its negative charge near these two pore-lining residues.

The protection of engineered cysteines by GlyH-101 might reflect the −1 charge on the blocker, a steric effect of the blocker, or some combination thereof. As a test for the role of charge-charge interactions, we compared the protection of the T338C CFTR against reactions with $MTSET^+$ and $MTSES^-$. The results summarized in Fig. 6 showed that the T338C CFTR was protected by GlyH-101 from negatively charged $MTSES^-$ but not from positively charged $MTSET^+$, indicating that the charge on the blocker is a major determinant of the protective effect at this position. This finding is consistent with our previously presented model for the pore, which places Thr338 on the outward-facing rim of the pore bottleneck, within the larger outer vestibule of the pore (Alexander et al., 2009; Norimatsu et al., 2012), where it would be less likely to be protected through steric restriction alone. We also studied the reaction of the I1131C CFTR with $MTSES^-$. In our molecular model, Ile1131 is predicted to lie within the outer vestibule of the pore but to occupy a position more distant from the negative charge of GlyH-101 than that of either Phe337 or Thr338 (Supplemental Fig. 2). This additional distance suggests less electrostatic protection of a cysteine at position 1131 by GlyH-101. No occlusion of I1131C was observed with 10 μM GlyH-101, despite more than 80% blockade of the I1131C CFTR current. The rate of reaction between $MTSES^-$ and the I1131C CFTR was actually somewhat greater in the presence of GlyH-101 (Fig. 7A).

The rates of reactions of charged reagents with the I1131C CFTR would be influenced by the relative positions of nearby charges, which might change slightly upon GlyH-101 binding. As shown in Supplemental Fig. 2, our molecular models of the CFTR predict one positively charged residue (Arg1128) and two negatively charged residues (Glu1124 and Glu1126) within 1 Debye length (9.2 Å) of position 1131. The electrostatic potential near an engineered cysteine thiolate is expected to influence the reaction rate of the cysteine with a thiol-reactive reagent in at least two ways: by altering the pK_a of the thiol group and by modifying the local concentration of the thiol-reactive reagent (Karlin and Akabas, 1998; Liu et al., 2004). The presence of negative charges near Ile1131 is consistent with the observed slow reaction of the I1131C CFTR with $MTSES^-$ (20 $M^{-1}\,s^{-1}$) (Fig. 7), which is more than 100-fold less than the rate seen with a cysteine at position 338 (3.3×10^3 $M^{-1}\,s^{-1}$) (Fig. 6). As reported previously (Norimatsu et al., 2012), the macroscopic conductance of the I1131C CFTR was increased by deposition of the negatively charged sulfonic acid group through reaction with $MTSES^-$. This result is most likely a reflection of an increase in the open probability of I1131C CFTR channels, similar to that observed for the R352C CFTR (Bai et al., 2010).

In the binding mode predicted for GlyH-101 (Fig. 2), a residue predicted to lie within the pore bottleneck, Ser341, is occluded by the bulk of the blocker, which suggests that a cysteine at this position should be at least partially protected from reactions with thiol-directed reagents in the presence of GlyH-101. A cysteine at position 341 is not reactive toward externally applied $MTSET^+$ or $MTSES^-$, however, presumably because these bulky polar reagents cannot enter the narrow portion of the pore from the outside (Norimatsu et al., 2012). The S341C CFTR is reactive toward channel-permeant reagents such as $[Ag(CN)_2]^-$ but the reactions at this position are not irreversible, which is a requirement for implementation of the post-GlyH-101 washout protocol. For this reason, we compared the reactivity of a cysteine at position 341 with the uncharged reagent NEM in the presence and absence of GlyH-101. NEM reacts irreversibly with a cys-

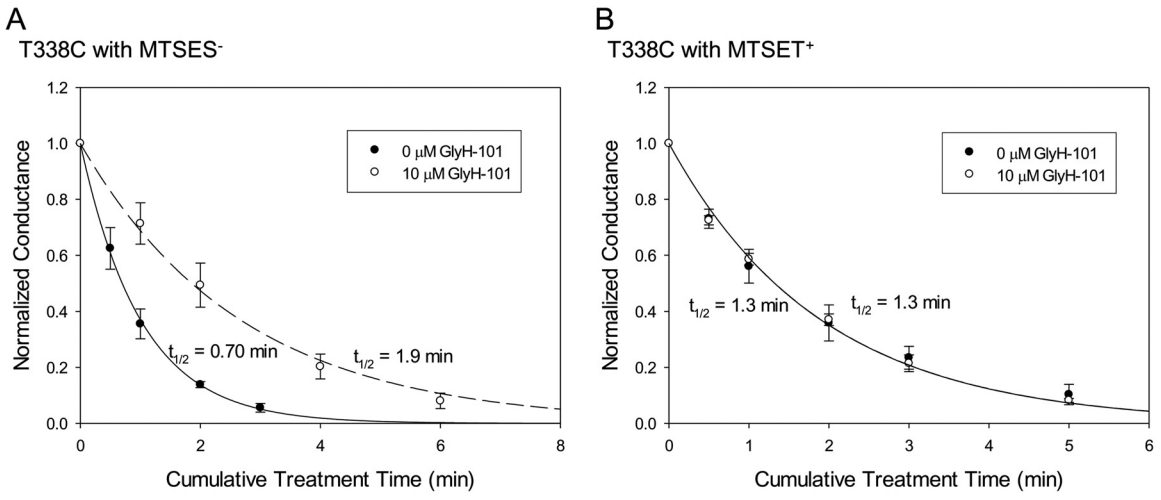

Fig. 6. GlyH-101 protection of T338C (an engineered cysteine at position 338) from $MTSES^-$ but not from $MTSET^+$. A, the T338C CFTR was reacted with 5 μM $MTSES^-$ in the presence and absence of 10 μM GlyH-101. Data points represent mean ± S.E.M. (n = 3). The lines represent the best fits of single-exponential functions to the conductance data. The half-life of each single-exponential fit is shown. The $MTSES^-$ reaction rate was almost 3 times slower in the presence of GlyH-101. The second-order reaction rate constants for $MTSES^-$ in the presence and absence of 10 μM GlyH-101 were 1.2×10^3 and 3.3×10^3 $M^{-1}\,s^{-1}$, respectively. B, the T338C CFTR was reacted with 50 μM $MTSET^+$ in the presence and absence of 10 μM GlyH-101. Data points represent mean ± S.E.M. (n = 3). The presence of GlyH-101 had no impact on the $MTSET^+$ reaction rate. The second-order reaction rate constants for $MTSET^+$ in the presence and absence of GlyH-101 were 1.8×10^2 $M^{-1}\,s^{-1}$.

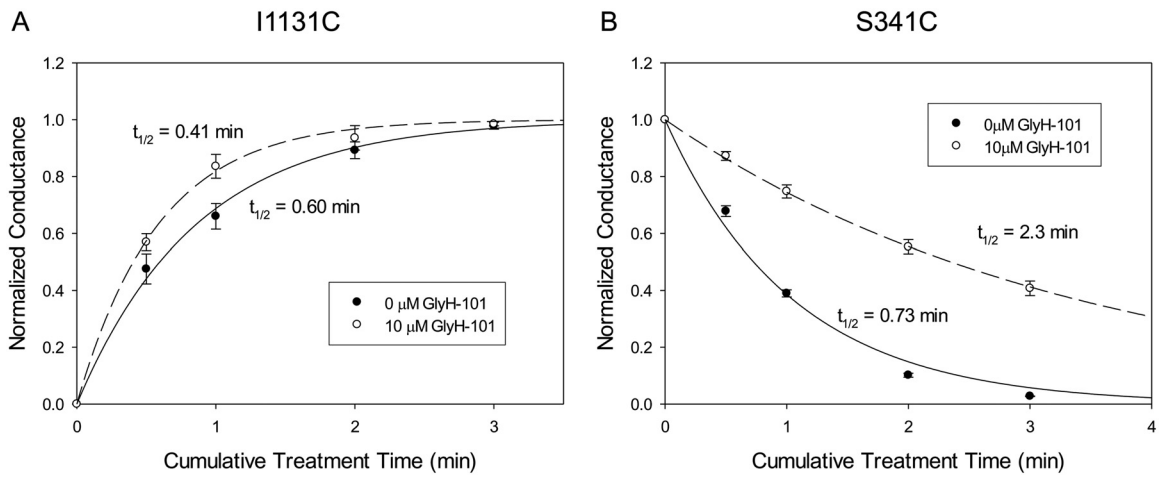

Fig. 7. A, time courses of the reactions of the I1131C CFTR with 1 mM $MTSES^-$ in the presence and absence of 10 μM GlyH-101. Data points represent mean ± S.E.M. (n = 3). Covalent labeling of the I1131C CFTR with $MTSES^-$ resulted in increases in conductance. The lines represent the best fits of single-exponential functions to the conductance data. The half-life of each single-exponential fit is shown. The second-order reaction rate constants in the presence and absence of 10 μM GlyH-101 were 28 and 20 M^{-1} s^{-1}, respectively. The EC_{50} at 0 mV for GlyH-101 blockade for the I1131C CFTR was 0.86 ± 0.016 μM (n = 3). B, time courses of the reactions of the S341C CFTR with 1 mM NEM in the presence and absence of 10 μM GlyH-101. Data points represent mean ± S.E.M. (n = 3). Covalent labeling of the S341C CFTR with NEM resulted in reductions in conductance. The lines represent the best fits of single-exponential functions to the conductance data. The half-life of each single-exponential fit is shown. The second-order reaction rate constants in the presence and absence of 10 μM GlyH-101 were 5.3 and 16 M^{-1} s^{-1}, respectively. The EC_{50} at 0 mV for GlyH-101 blockade for the S341C CFTR was 0.89 ± 0.056 μM (n = 3).

teine at position 341 and reduces conductance to nearly 0 (Supplemental Fig. 3). The data in Fig. 7B indicate that GlyH-101 protected the cysteine at position 341 from reaction with NEM, which is consistent with a cork-in-the-bottle type of obstruction of the pore bottleneck. We could not determine with certainty the exact route by which externally applied NEM reaches the cysteine at position 341, i.e., by traversing the outer vestibule and entering the pore bottleneck or by taking a more-circuitous path through the lipid bilayer, which reflects the membrane permeability of this compound (Lê-Quôc et al., 1981). In either case, the presence of GlyH-101 in the proposed binding site is predicted to obstruct the access of NEM to the cysteine thiolate.

The GlyH-101 EC_{50} Is Reduced Approximately 200-Fold with F342A CFTR. The binding mode predicted for GlyH-101 drew our attention to another residue that is predicted to lie within the pore bottleneck, Phe342. A cysteine at this position was reactive toward the channel-permeant, thiol-directed reagent $[Ag(CN)_2]^-$ but not the larger reagents $MTSET^+$ and $MTSES^-$ applied from the extracellular side of the channel. This result suggested that the residue formed part of the lining of the narrow region of the pore (Alexander et al., 2009). The bulky side chain of Phe342 appeared to impinge on the docked GlyH-101; in principle, this juxtaposition might lead to a favorable π-π interaction (Meyer et al., 2003; Paton and Goodman, 2009) or a steric obstruction that would be unfavorable to GlyH-101 binding. We analyzed GlyH-101 binding to wt and F342A CFTR channels by using the MM-GB/SA method described by Guimarães and Cardozo (2008). To predict the structure of the F342A CFTR–GlyH-101 complex, the phenylalanine at position 342 of the wt CFTR was mutated to alanine in silico (see *Materials and Methods*) and GlyH-101 was docked to the mutant CFTR by using IFD techniques (Supplemental PDB File 3). The MM-GB/SA method estimates the free energy of binding, ΔG_{bind}, by computing its components described by eq. 1. The estimated parameter values for wt and F342A CFTRs are presented in Table 2. The calculations suggested that the free energy of binding of GlyH-101, ΔG_{bind}, is more negative for the F342A CFTR than for the wt CFTR, that is, the F342A CFTR binds GlyH-101 more tightly than does the wt CFTR. Examination of the total binding free energy according to the terms listed in eq. 1 revealed that the predicted energy difference arises mainly from reduction of the strain energy of

TABLE 2

GlyH-101 binding free energy, ΔG_{bind}, and its components estimated through MM-GB/SA analysis for wt and F342A CFTRs, without and with a membrane

Analyses were performed with eq. 1, $\Delta G_{bind} = \Delta E_{lig} + \Delta G_{solv} - T\Delta S_{conf} + E_{vdw} + E_{es} + \Delta E_{PTN}$, where ΔE_{lig} and ΔE_{PTN} are changes (upon ligand binding) in the intramolecular strains of the ligand and protein, respectively, ΔG_{solv} is the total desolvation penalty for the ligand and protein, $T\Delta S_{conf}$ is the ligand conformational penalty, and E_{vdw} and E_{es} are the van der Waals and electrostatic energies, respectively.

CFTR	ΔE_{lig}	ΔE_{PTN}	$E_{vdw} + E_{es} + \Delta G_{solv}$	$-T\Delta S_{conf}$	ΔG_{bind}
	kcal/mol	*kcal/mol*	*kcal/mol*	*kcal/mol*	*kcal/mol*
Without membrane					
wt	4.68	6.89	−21.2	1.05	−8.54
F342A	3.90	4.04	−21.6	1.05	−12.6
wt − F342A	0.78	2.85	0.42	0.0	4.0
With membrane					
wt	4.68	6.88	−19.8	1.05	−7.23
F342A	3.92	4.05	−20.4	1.05	−11.4
wt − F342A	0.76	2.82	0.54	0.0	4.1

the F342A CFTR (E_{PTN}), consistent with the notion that the side chain of Phe342 in the wt CFTR channel causes an unfavorable steric clash with GlyH-101. Calculations were performed with the absence and presence of a lipid membrane, but the presence of a membrane had a relatively small effect on the free energy calculation. The calculated free energies of GlyH-101 binding were −7.43 and −8.54 kcal/mol for the wt CFTR and −11.8 and −12.6 kcal/mol for the F342A CFTR with and without the membrane, respectively.

The experimental results presented in Fig. 8A showed that dose-dependent blockade of the F342A CFTR by GlyH-101, as predicted by the MM-GB/SA analysis, exhibited an $EC_{50}(0)$ that was dramatically reduced (5.2 ± 0.83 nM; n = 3), compared with that of the wt CFTR (1.1 ± 0.11 μM; n = 4) (Fig. 1C), which is consistent with a substantial increase in binding affinity for the blocker with elimination of the bulky phenylalanine side chain. The substantially higher apparent affinity of the F342A CFTR for GlyH-101 suggests dramatic slowing of the off-rate for the bound blocker. This prediction was confirmed in experiments such as those illustrated in Fig. 8, B and C, in which we measured the time course of the changes in channel blockade in response to voltage steps. A negative voltage step would be expected to drive the bound blocker off the binding site, whereas a positive voltage step would be expected to drive the blocker into the binding site. In the representative experiment depicted in Fig. 8C, 100 nM GlyH-101 was present in the bath and the voltage was held initially at 0 mV to allow equilibration of the blocker with the binding site. When the voltage was stepped to negative values, the time course of the recovery of current could be monitored as the blocker was driven off the binding site. This was followed by a voltage step to +40 mV so that the time course of the enhanced blockade of current could be monitored as the blocker was driven into the binding site. The change in channel blockade during a voltage step was too fast to be measured for the wt CFTR (Supplemental Fig. 4), but a single-exponential time course was easily resolved for the high-affinity mutant. Experiments of this type that were performed with different concentrations of GlyH-101 enabled us to determine the single-exponential relaxation rate (the reciprocal of the time constant of the relaxation) at different membrane potential values. This rate, k_{Gly}, is the sum of the on- and off-rates; i.e., $k_{Gly} = k'_{on}[GlyH] + k_{off}$, where k'_{on} is the second-order rate constant for blocker binding, [GlyH] is the concentration of GlyH-101, and k_{off} is the dissociation rate constant. Values for k'_{on} and k_{off} were obtained from plots like those shown in Fig. 8D, in which k_{Gly} is plotted versus the GlyH-101 concentration. Consistent with eq. 3, the relaxation rates exhibited linear dependence on the concentration of GlyH-101. Whereas both k'_{on} and k_{off} were voltage-dependent for glibenclamide binding (Zhou et al., 2002; Zhang et al., 2004a,b), only k_{off} displayed voltage dependence for GlyH-101 binding, which suggests that the main energy barrier to GlyH-101 entry into the pore bottleneck lies outside or near the edge of the electric field. Values for k'_{on} ($2.3 \times 10^7\ M^{-1}\ s^{-1}$) and k_{off} ($0.088\ s^{-1}$ at 0 mV) (Fig. 8, E and F) yielded an estimated K_D at 0 mV of ~4 nM, close to the value of $EC_{50}(0)$ determined from the dose-response analysis of steady-state blockade (5.2 nM). The k'_{on} of GlyH-101 for the wt CFTR could be calculated from the mean open lifetime of the channel in the presence of GlyH-101, as observed by Muanprasat et al. (2004) in single-channel recordings. With the data reported by those authors, the k'_{on} for the wt CFTR was calculated to be $1.6 \times 10^7\ M^{-1}\ s^{-1}$, a value similar to the k'_{on} for the F342A CFTR ($2.3 \times 10^7\ M^{-1}\ s^{-1}$) determined in the current study, which indicates that the difference in EC_{50} values between the wt and F342A CFTRs is attributable to the slow off-rate of GlyH-101 with the F342A CFTR. The binding free energy values based on the observed EC_{50} values, estimated as $RT\ln(EC_{50})$, were −8.12 kcal/mol for the wt CFTR and −11.3 kcal/mol for the F342A CFTR. These empirical values are qualitatively consistent with the computed free energies obtained by applying the MM-GB/SA technique to the proposed model of GlyH-101 binding (Fig. 2) for the wt CFTR (−7.43 kcal/mol) and the F342A CFTR (−11.8 kcal/mol).

Discussion

GlyH-101 Binds in the Bottleneck of the CFTR Pore. The results presented here identify a plausible binding mode for the pore blocker GlyH-101. Molecular modeling and experimental assay results are consistent with the notion that GlyH-101 blocks anion conduction by entering the CFTR channel from the external solution, passing through the outer vestibule, and then lodging in the mouth of a narrow bottleneck in the pore. This model is consistent with previous findings by Muanprasat et al. (2004) that indicated that GlyH-101 is an open-channel blocker that enters the CFTR channel from the extracellular side and with studies by Sonawane et al. (2006, 2007) that showed that GlyH-101 analogs rendered membrane-impermeant and channel-impermeant through conjugation with polyethylene glycol and lectin also blocked the CFTR channel from the extracellular side. In the predicted binding mode, the hydrophobic tail of GlyH-101 inserts into the pore bottleneck such that the entrance to the bottleneck is partially occluded and the charged end of the molecule resides near two TM6 residues within the outer vestibule of the pore, i.e., Phe337 and Thr338.

The predicted binding mode for GlyH-101 is in accord with three experimental observations presented here. First, reactions of thiol-directed probes with cysteines substituted at positions 337 and 338, which occur predominantly in the open conformation of the channel, were occluded when GlyH-101 was within the channel. For position 338, this occluding effect was attributable primarily to the net negative charge in the portion of GlyH-101 that protrudes into the outer vestibule. An occluding effect was not observed for a cysteine substituted at the more-distant position 1131 (Fig. 7A). GlyH-101 also occluded the reaction of the neutral reagent NEM with a cysteine at position 341, which is consistent with the notion that position 341 lies within the narrow region of the pore, where a cork-in-the-bottle effect would be expected to reduce the access of an uncharged thiol-directed probe regardless of its route of access. Second, alkylation of the T338C CFTR with iodoacetamide, which results in covalent addition of an acetamide moiety that is predicted by the model to create a steric clash with GlyH-101, significantly reduced the apparent binding affinity of GlyH-101. In contrast, alkylation of the F337C CFTR with iodoacetamide was not predicted by the molecular model to cause a steric clash and did not alter GlyH-101 blockade markedly. Finally, when a predicted steric clash between the side chain of Phe342 and the naphthalene tail of the bound blocker was removed through mutation of the residue to an alanine (F342A), the

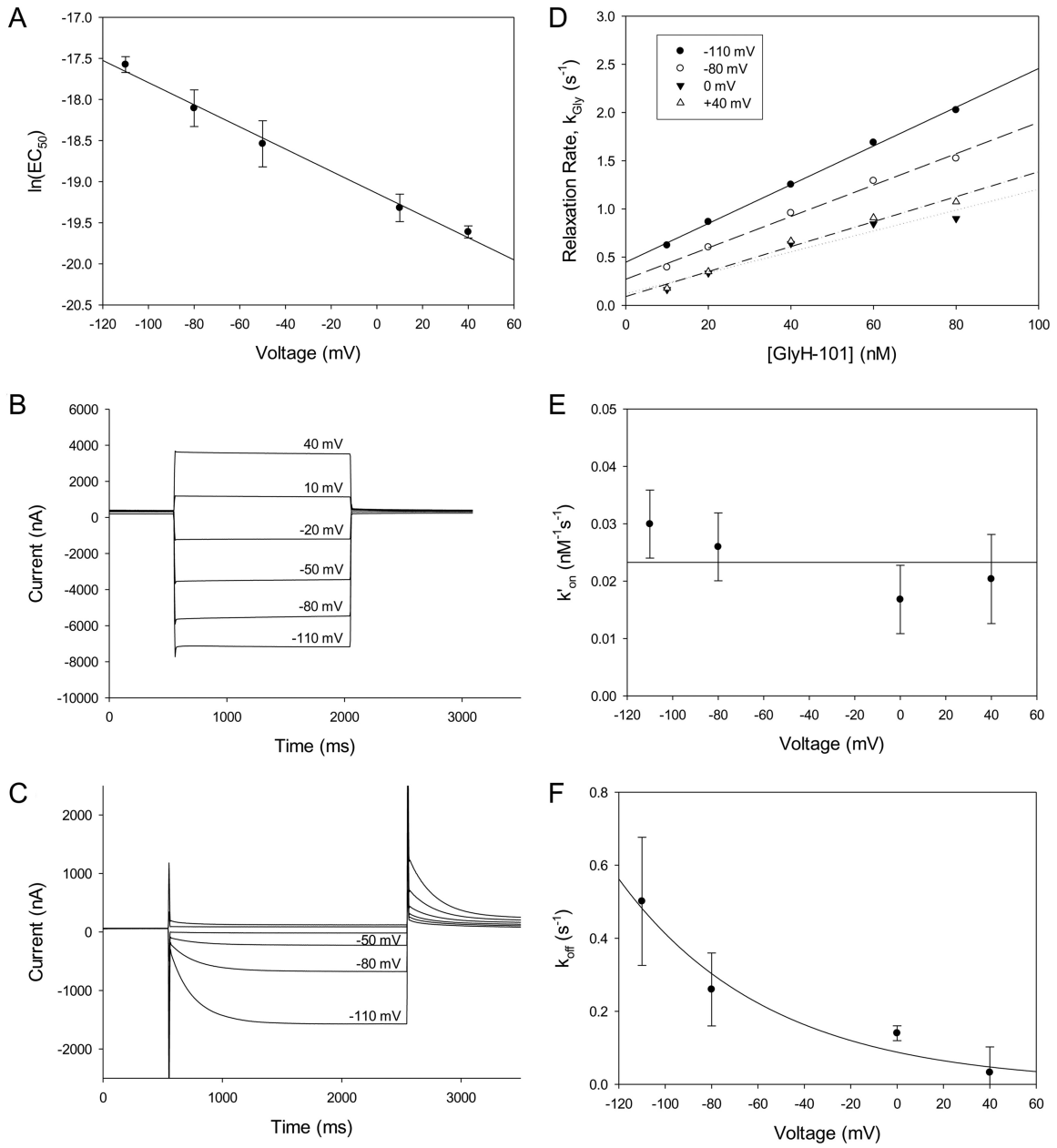

Fig. 8. F342A CFTR transmembrane currents. F342A CFTR channels were expressed in *Xenopus laevis* oocytes, and transmembrane currents were measured at clamped voltages by using a two-electrode, voltage-clamp technique. A, the voltage dependence of the GlyH-101 EC_{50} for the F342A CFTR is consistent with the Woodhull model (Woodhull, 1973; Tikhonov and Magazanik, 1998), in a manner similar to that of wt CFTR (Fig. 1). Data points represent mean ± S.E.M. ($n = 3$). The EC_{50} at 0 mV was 5.2 ± 0.83 nM ($n = 3$), and the apparent electrical distance was 0.35 ± 0.019 ($n = 3$). B, the channels were activated with a stimulating cocktail containing isoproterenol and IBMX. Six current traces were recorded in the absence of GlyH-101 and are shown superimposed. At the beginning of each trace, the voltage was held at 0 mV for 0.5 s; it was then stepped to −110, −80, −50, −20, +10, or +40 mV for 1.5 s. After this step, the voltage was held at 0 mV for 1 s. C, GlyH-101 was applied to the same oocyte as used in B. Six traces were recorded in the presence of 100 nM GlyH-101 and are shown superimposed. At the beginning of each trace, the voltage was held at 0 mV for 0.5 s; it was then stepped to −110, −80, −50, −20, +10, or +40 mV for 2 s. After this step, the voltage was held at +40 mV for 5 s. D, the rates of single-exponential time courses shown in B were plotted against the concentration of GlyH-101. The relaxation rate (the reciprocal of the time constant for the single-exponential relaxation) exhibited a linear dependence on the GlyH-101 concentration. As described by eq. 3, the second-order binding rate constant k'_{on} and the off-rate k_{off} could be determined from the best-fit line. E, the second-order binding rate constant k'_{on} values (mean ± S.E.M.; $n = 3$) were plotted against the transmembrane voltage. The data were fit by using the equation $k'_{on}(V) = k'_{on}(0)\exp(\delta_b FV/RT)$, where δ_b is the voltage dependence constant for k'_{on} and F, R, and T have their usual meanings (Tikhonov and Magazanik, 1998); $k'_{on}(0)$ was estimated to be $2.3 \times 10^7\ M^{-1}\ s^{-1}$. F, the off-rates (mean ± S.E.M.; $n = 3$) were plotted against the transmembrane voltage. The data were fit by using the equation $k_{off}(V) = k_{off}(0)\exp(-\delta FV/RT)$, where δ is the voltage dependence constant for k_{off} and F, R, and T have their usual meanings (Tikhonov and Magazanik, 1998); $k_{off}(0)$ was estimated to be $0.088\ s^{-1}$.

apparent blocker affinity was increased more than 200-fold, a change consistent with the free energies of binding estimated using a MM-GB/SA approach.

The proposed mode of GlyH-101 binding is reminiscent of glibenclamide blockade of the CFTR, for which it was suggested that the charged sulfonylurea moiety and the benzamide group of the blocker molecule interact with different parts of the CFTR pore (Cai et al., 1999; Zhang et al., 2004b).

In the case of GlyH-101, the combination of the charged head and the naphthalene tail is required for potent blockade. The EC_{50} increases to more than 50 μM if the charged dibromodihydroxylphenyl head or the naphthalene tail is substituted with a benzene ring (Muanprasat et al., 2004). Although glibenclamide has multiple binding sites and shows complex binding kinetics, the blockade is dominated by the binding site with the slowest off-rate (Zhang et al., 2004a). The k'_{on} of GlyH-101 for the wt CFTR (1.6×10^7 M^{-1} s^{-1}) (Muanprasat et al., 2004) is much greater than that of glibenclamide ($\sim 2 \times 10^5$ M^{-1} s^{-1}) (Zhou et al., 2002), whereas the off-rates of the two molecules are similar (10–26 s^{-1}) (Zhou et al., 2002; Muanprasat et al., 2004; Zhang et al., 2004b), which suggests that the greater potency of GlyH-101 for the wt CFTR [$EC_{50}(0) = 1.1$ μM], in comparison with that of glibenclamide (EC_{50} of ~ 50 μM at -60 mV) (Zhou et al., 2002), is attributable mainly to the difference in k'_{on} values.

State-Dependent Cysteine Reactivity Suggests Movements of the Outer Vestibule of the Pore. The results presented in the current study provide evidence for strong state dependence of the rates of reactions of externally applied, thiol-directed probes with cysteines substituted at positions 337 and 338. In both cases, reactions were favored by a factor of at least 20 in channels activated by increases in cytosolic cAMP levels. In view of our finding that the preactivation closed state is operationally equivalent to the closed state that is visited transiently during the gating cycle, after channel activation, these results argue for an open outer vestibule in the conducting state of the CFTR pore, as predicted by our Sav1866-based homology model (Norimatsu et al., 2012). The state-dependent reactivity of the T338C CFTR that was observed in the current study is consistent with the finding by Beck et al. (2008) that $MTSES^-$ reacted slightly faster with a mutant with high open probability (T338C/E1371Q CFTR) than with the T338C/wt CFTR.[2]

Mornon et al. (2009) created a homology model of the CFTR that was based on the inward-facing conformation of the prokaryotic transporter MsbA (PDB code 3B5X) (Ward et al., 2007). In this crystal structure, the nucleotide-binding domains of MsbA are partially dissociated, a conformation that is generally associated with the nonconducting state of the CFTR channel. Comparison of this model with our Sav1866-based model suggests the possibility of dramatic movement in the region around Phe337 and Thr338 during the transition between the open and closed states. Whereas Phe337 and Thr338 are accessible to the aqueous environment in our Sav1866-based model (Norimatsu et al., 2012), these residues are predicted to be occluded by surrounding residues in the MsbA-based model described by Mornon et al. (2009) (Fig. 9). A conformational change of this sort would be consistent with the state-dependent reactivity of the F337C and T338C CFTRs observed in the current study. The MsbA-based model described by Mornon et al. (2009) also suggests that the side chain of Arg334 protrudes into the external aqueous environment; when Arg334 is mutated to a cysteine

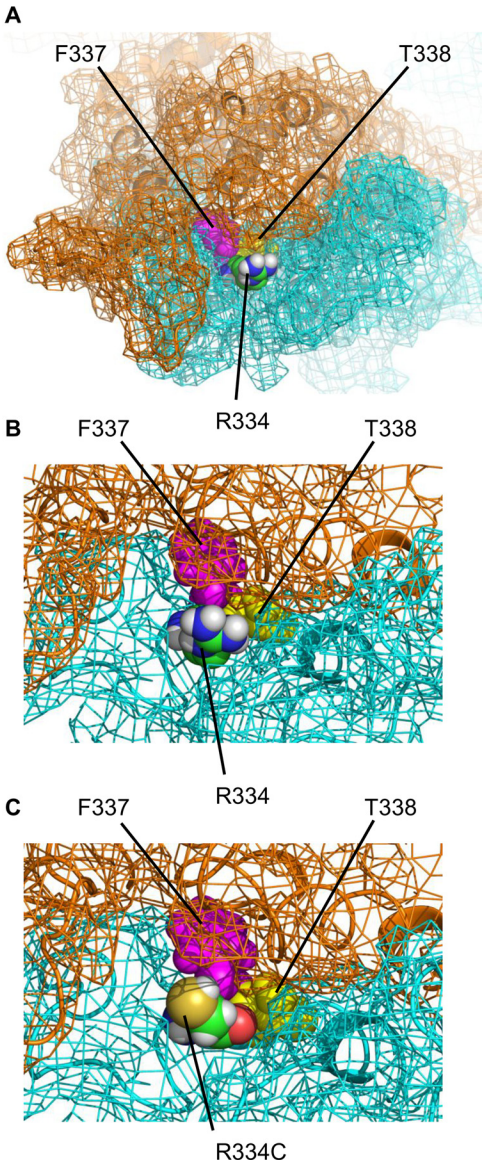

Fig. 9. Homology model of the CFTR based on MsbA (Mornon et al., 2009). A, top view from the extracellular side. Arg334, Phe337, and Thr338 are shown as van der Waals representations. The carbon atoms of Thr334 are colored green, and Phe337 and Thr338 are colored pink and yellow, respectively. B, close-up view of the structure shown in A, around Thr334. The CFTR molecule is shown as a cartoon representation, with its molecular surface indicated by mesh. Transmembrane domain 1 is shown in cyan and transmembrane domain 2 in orange. C, view with Thr334, shown in B, mutated to cysteine with Maestro 9.1 (Schrödinger).

[2] The findings presented here regarding the state-dependent reactivity of engineered cysteines are at odds with previous reports (Wang and Linsdell, 2012; Fatehi and Linsdell, 2008). Wang and Linsdell (2012) studied reactions of the T338C/E1371Q CFTR with $MTSES^-$ and $[Au(CN)_2]^-$ and suggested that the reaction of an engineered cysteine at position 338 with externally applied reagents was favored in the closed state. However, this observation conflicts with that by Beck et al. (2008), who reported that $MTSES^-$ reacted slightly faster with a double-mutant with high open probability (T338C/E1371Q CFTR) than with the T338C/wt CFTR. We observed reaction rates for $MTSES^-$ with T338C/wt and T338C/E1371Q CFTRs that were similar to those observed by Beck et al. (2008) (data not shown), which supports the idea that the T338C CFTR reacts in the open state. Fatehi and Linsdell (2008) reported, contrary to our findings, that reactions of $MTSES^-$ and $[Au(CN)_2]^-$ with a cysteine at position 334 were favored in the activated state of the channel. Cells expressing the R334C CFTR were preincubated with $MTSES^-$ with and without an activating cocktail of forskolin and IBMX, and the reaction, which was inferred on the basis of changes in the rectification ratio of the CFTR *I-V* curve, was observed only with cells exposed to the activating cocktail. However, the differences observed between cells incubated with or without $MTSES^-$ or with or without the activating cocktail were very subtle, and such changes easily could result from metal contamination (Liu et al., 2006; Liu, 2008), which was not controlled in that study. Similarly, the outcome of cell preincubation with $[Au(CN)_2]^-$ and the subsequent reversal of CFTR blockade by CN^- can be influenced by metal contamination and the redox state of the cell (Liu, 2008). It is possible that the state dependence observed by Fatehi and Linsdell (2008) was attributable to such an artifact.

with Maestro 9.1 (Schrödinger) in the MsbA-based model, the reactive thiolate is clearly accessible from the extracellular solution (Fig. 9C), which is consistent with the closed-state reactivity of R334C observed in the current study and in the study by Zhang et al. (2005). The mechanism that renders the R334C CFTR unreactive in the conducting state is not clear. When Arg334 is mutated to a cysteine with Maestro 9.1 in the snapshots from our MD simulation (Norimatsu et al., 2012), the thiol group is clearly accessible from the external solution in all of the snapshots. The R334C mutation may cause significant conformational changes in the CFTR protein (that are not captured in our MD simulation), as suggested by Zhou et al. (2007), which render the engineered cysteine inaccessible in the conducting state of the CFTR.

GlyH-101 Docking Is a Test of the Sav1866-Based Model of the Pore. In the absence of a reported crystal structure, homology models of the CFTR provide the only means by which the effects of point mutations or chemical modifications can be interpreted in a structural context. Low levels of homology between the template protein (in this case, Sav1866) and the CFTR, however, require that any such model be tested extensively. Dalton et al. (2012) used a Sav1866-based homology model of the CFTR to identify potential binding modes for pore-blocking molecules thought to access the channel from the cytosolic side, but neither the model nor the predicted blocker binding modes were experimentally verified. In previous studies, we used several approaches to test the predictions of our Sav1866-based molecular models. Cysteine scanning was used to identify pore-lining residues in TMs 6, 12, 3, and 9. Levels of agreement with model predictions for side chain orientations ranged from 77 to 90% (Norimatsu et al., 2012). We compared the patterns of reactivity of cysteines engineered into the two primary pore-lining helices, i.e., TM6 and TM12, toward channel-permeant and channel-impermeant, thiol-directed probes. The observed patterns of reactivity located the outer boundary of a narrow bottleneck in the pore to a short segment between Thr338 and Ser341, the location predicted by the Sav1866-based model. Finally, we used the motion of the transmembrane segments inferred from MD simulations to predict the transient formation of a salt bridge, which had been postulated by Cui et al. (2008) on the basis of the effects of charge substitutions on single-channel behavior. The agreement between the predicted binding mode of the open-channel blocker GlyH-101 in the narrow region of the CFTR pore and the experimental observations reported here suggests that more-stringent tests of homology models can be based on locating binding sites for multiple small molecules within the pore. With further refinement, the Sav1866-based model (or its descendents) should be a useful template for in silico screening of compound libraries.

Acknowledgments

We are very grateful to Drs. Alan Verkman, Nitin Sonawane, and Robert Bridges (Cystic Fibrosis Foundation Therapeutics) for the generous provision of samples of GlyH-101 used in these studies.

Authorship Contributions

Participated in research design: Norimatsu and Dawson.
Conducted experiments: Norimatsu, Alexander, and O'Donnell.
Performed data analysis: Norimatsu, Ivetac, Frye, and Sansom.
Wrote or contributed to the writing of the manuscript: Norimatsu and Dawson.

Appendix

The thiol modification rate constant, before or after activation, can be expressed as a weighted average of the modification rates for open and closed channels, $\kappa_{ob} = f_c \times \kappa_c + (1 - f_c) \times \kappa_o$ (eq. 2), where κ_{ob} is the observed reaction rate constant, f_c is the closed probability of the channels, and κ_c and κ_o are the reaction rate constants for the closed and open channels, respectively.

With the assumption of $\kappa_o = 0$, $\kappa_{ob} = f_c \times \kappa_c$ before activation of the CFTR channels. After activation, $k'_{ob} = f'_c \times \kappa_c$, where f'_c is the postactivation closed probability. Therefore, $\kappa_{ob}/k'_{ob} = (f_c \times \kappa_c)/(f'_c \times \kappa_c)$. With $MTSET^+$, $\kappa_{ob} = 7.2 \times 10^4\ M^{-1}\ s^{-1}$, $k'_{ob} = 3.9 \times 10^4\ M^{-1}\ s^{-1}$, and κ_{ob}/k'_{ob} is ~1.9. With $[Au(CN)_2]^-$, $\kappa_{ob} = 8.9 \times 10^2\ M^{-1}\ s^{-1}$, $k'_{ob} = 2.6 \times 10^2\ M^{-1}\ s^{-1}$, and κ_{ob}/k'_{ob} is ~3.5. The closed probability of the channels before activation, f_c, is close to 1. Because we observed experimentally more than 100-fold increases in macroscopic conductance during channel activation, f_c was estimated to be >0.99. With the substitution of 1.9 for κ_{ob}/k'_{ob} and 1 for f_c, the postactivation closed probability, f'_c, is ~0.5; with the substitution of 3.5 for κ_{ob}/k'_{ob} and 1 for f_c, f'_c is ~0.3. Therefore, the postactivation closed probability is ~0.3 to 0.5 and the open probability is ~0.5 to 0.7.

References

Alexander C, Ivetac A, Liu X, Norimatsu Y, Serrano JR, Landstrom A, Sansom M, and Dawson DC (2009) Cystic fibrosis transmembrane conductance regulator: using differential reactivity toward channel-permeant and channel-impermeant thiol-reactive probes to test a molecular model for the pore. *Biochemistry* **48:** 10078–10088.

Bai Y, Li M, and Hwang TC (2010) Dual roles of the sixth transmembrane segment of the CFTR chloride channel in gating and permeation. *J Gen Physiol* **136:**293–309.

Beck EJ, Yang Y, Yaemsiri S, and Raghuram V (2008) Conformational changes in a pore-lining helix coupled to cystic fibrosis transmembrane conductance regulator channel gating. *J Biol Chem* **283:**4957–4966.

Bompadre SG, Ai T, Cho JH, Wang X, Sohma Y, Li M, and Hwang TC (2005) CFTR gating I: characterization of the ATP-dependent gating of a phosphorylation-independent CFTR channel (ΔR-CFTR). *J Gen Physiol* **125:**361–375.

Boucher RC (2007) Airway surface dehydration in cystic fibrosis: pathogenesis and therapy. *Annu Rev Med* **58:**157–170.

Cai Z, Lansdell KA, and Sheppard DN (1999) Inhibition of heterologously expressed cystic fibrosis transmembrane conductance regulator Cl^- channels by non-sulphonylurea hypoglycaemic agents. *Br J Pharmacol* **128:**108–118.

Cai Z, Scott-Ward TS, and Sheppard DN (2003) Voltage-dependent gating of the cystic fibrosis transmembrane conductance regulator Cl^- channel. *J Gen Physiol* **122:**605–620.

Carra C, Saha J, and Cucinotta FA (2012) Theoretical prediction of the binding free energy for mutants of replication protein A. *J Mol Model* **18:**3035–3049.

Csanády L, Vergani P, and Gadsby DC (2010) Strict coupling between CFTR's catalytic cycle and gating of its Cl^- ion pore revealed by distributions of open channel burst durations. *Proc Natl Acad Sci USA* **107:**1241–1246.

Cui G, Song B, Turki HW, and McCarty NA (2012) Differential contribution of TM6 and TM12 to the pore of CFTR identified by three sulfonylurea-based blockers. *Pflugers Arch* **463:**405–418.

Cui G, Zhang ZR, O'Brien AR, Song B, and McCarty NA (2008) Mutations at arginine 352 alter the pore architecture of CFTR. *J Membr Biol* **222:**91–106.

Dailey MM, Hait C, Holt PA, Maguire JM, Meier JB, Miller MC, Petraccone L, and Trent JO (2009) Structure-based drug design: from nucleic acid to membrane protein targets. *Exp Mol Pathol* **86:**141–150.

Dalton J, Kalid O, Schushan M, Ben-Tal N, and Villà-Freixa J (2012) New model of cystic fibrosis transmembrane conductance regulator proposes active channel-like conformation. *J Chem Inf Model* **52:**1842–1853.

de Hostos EL, Choy RK, and Nguyen T (2011) Developing novel antisecretory drugs to treat infectious diarrhea. *Future Med Chem* **3:**1317–1325.

del Camino D, Holmgren M, Liu Y, and Yellen G (2000) Blocker protection in the pore of a voltage-gated K^+ channel and its structural implications. *Nature* **403:**321–325.

Fatehi M and Linsdell P (2008) State-dependent access of anions to the cystic fibrosis transmembrane conductance regulator chloride channel pore. *J Biol Chem* **283:** 6102–6109.

Fischer H and Machen TE (1994) CFTR displays voltage dependence and two gating modes during stimulation. *J Gen Physiol* **104:**541–566.

Friesner RA, Murphy RB, Repasky MP, Frye LL, Greenwood JR, Halgren TA,

Sanschagrin PC, and Mainz DT (2006) Extra precision glide: docking and scoring incorporating a model of hydrophobic enclosure for protein-ligand complexes. *J Med Chem* **49:**6177–6196.
Guimarães CR and Cardozo M (2008) MM-GB/SA rescoring of docking poses in structure-based lead optimization. *J Chem Inf Model* **48:**958–970.
Holmgren M, Liu Y, Xu Y, and Yellen G (1996) On the use of thiol-modifying agents to determine channel topology. *Neuropharmacology* **35:**797–804.
Hwang TC and Sheppard DN (1999) Molecular pharmacology of the CFTR Cl^- channel. *Trends Pharmacol Sci* **20:**448–453.
Karlin A and Akabas MH (1998) Substituted-cysteine accessibility method. *Methods Enzymol* **293:**123–145.
Lê-Quôc K, Lê-Quôc D, and Gaudemer Y (1981) Evidence for the existence of two classes of sulfhydryl groups essential for membrane-bound succinate dehydrogenase activity. *Biochemistry* **20:**1705–1710.
Linsdell P (2005) Location of a common inhibitor binding site in the cytoplasmic vestibule of the cystic fibrosis transmembrane conductance regulator chloride channel pore. *J Biol Chem* **280:**8945–8950.
Liu X (2008) A possible role for intracellular GSH in spontaneous reaction of a cysteine (T338C) engineered into the cystic fibrosis transmembrane conductance regulator. *Biometals* **21:**277–287.
Liu X, Alexander C, Serrano J, Borg E, and Dawson DC (2006) Variable reactivity of an engineered cysteine at position 338 in cystic fibrosis transmembrane conductance regulator reflects different chemical states of the thiol. *J Biol Chem* **281:** 8275–8285.
Liu X, Smith SS, Sun F, and Dawson DC (2001) CFTR: covalent modification of cysteine-substituted channels expressed in *Xenopus* oocytes shows that activation is due to the opening of channels resident in the plasma membrane. *J Gen Physiol* **118:**433–446.
Liu X, Zhang ZR, Fuller MD, Billingsley J, McCarty NA, and Dawson DC (2004) CFTR: a cysteine at position 338 in TM6 senses a positive electrostatic potential in the pore. *Biophys J* **87:**3826–3841.
Mansoura MK, Smith SS, Choi AD, Richards NW, Strong TV, Drumm ML, Collins FS, and Dawson DC (1998) Cystic fibrosis transmembrane conductance regulator (CFTR) anion binding as a probe of the pore. *Biophys J* **74:**1320–1332.
Mense M, Vergani P, White DM, Altberg G, Nairn AC, and Gadsby DC (2006) In vivo phosphorylation of CFTR promotes formation of a nucleotide-binding domain heterodimer. *EMBO J* **25:**4728–4739.
Meyer EA, Castellano RK, and Diederich F (2003) Interactions with aromatic rings in chemical and biological recognition. *Angew Chem Int Ed Engl* **42:**1210–1250.
Mornon JP, Lehn P, and Callebaut I (2009) Molecular models of the open and closed states of the whole human CFTR protein. *Cell Mol Life Sci* **66:**3469–3486.
Muanprasat C, Sonawane ND, Salinas D, Taddei A, Galietta LJ, and Verkman AS (2004) Discovery of glycine hydrazide pore-occluding CFTR inhibitors: mechanism, structure-activity analysis, and in vivo efficacy. *J Gen Physiol* **124:**125–137.
Norimatsu Y, Ivetac A, Alexander C, Kirkham J, O'Donnell N, Dawson DC, and Sansom MS (2012) Cystic fibrosis transmembrane conductance regulator: a molecular model defines the architecture of the anion conduction path and locates a "bottleneck" in the pore. *Biochemistry* **51:**2199–2212.
Parker MH, Lunney EA, Ortwine DF, Pavlovsky AG, Humblet C, and Brouillette CG (1999) Analysis of the binding of hydroxamic acid and carboxylic acid inhibitors to the stromelysin-1 (matrix metalloproteinase-3) catalytic domain by isothermal titration calorimetry. *Biochemistry* **38:**13592–13601.
Paton RS and Goodman JM (2009) Hydrogen bonding and pi-stacking: how reliable are force fields? A critical evaluation of force field descriptions of nonbonded interactions. *J Chem Inf Model* **49:**944–955.
Rao S, Sanschagrin PC, Greenwood JR, Repasky MP, Sherman W, and Farid R (2008) Improving database enrichment through ensemble docking. *J Comput Aided Mol Des* **22:**621–627.
Riordan JR (2008) CFTR function and prospects for therapy. *Annu Rev Biochem* **77:**701–726.
Sanchez J and Holmgren J (2011) Cholera toxin: a foe & a friend. *Indian J Med Res* **133:**153–163.
Serrano JR, Liu X, Borg ER, Alexander CS, Shaw CF III, and Dawson DC (2006) CFTR: ligand exchange between a permeant anion ($[Au(CN)_2]^-$) and an engineered cysteine (T338C) blocks the pore. *Biophys J* **91:**1737–1748.
Sheppard DN (2004) CFTR channel pharmacology: novel pore blockers identified by high-throughput screening. *J Gen Physiol* **124:**109–113.
Sheppard DN and Robinson KA (1997) Mechanism of glibenclamide inhibition of cystic fibrosis transmembrane conductance regulator Cl^- channels expressed in a murine cell line. *J Physiol* **503:**333–346.
Sherman W, Beard HS, and Farid R (2006) Use of an induced fit receptor structure in virtual screening. *Chem Biol Drug Des* **67:**83–84.
Shoichet BK and Kobilka BK (2012) Structure-based drug screening for G-protein-coupled receptors. *Trends Pharmacol Sci* **33:**268–272.
Smith SS, Liu X, Zhang ZR, Sun F, Kriewall TE, McCarty NA, and Dawson DC (2001) CFTR: covalent and noncovalent modification suggests a role for fixed charges in anion conduction. *J Gen Physiol* **118:**407–431.
Sonawane ND, Hu J, Muanprasat C, and Verkman AS (2006) Luminally active, nonabsorbable CFTR inhibitors as potential therapy to reduce intestinal fluid loss in cholera. *FASEB J* **20:**130–132.
Sonawane ND, Zhao D, Zegarra-Moran O, Galietta LJ, and Verkman AS (2007) Lectin conjugates as potent, nonabsorbable CFTR inhibitors for reducing intestinal fluid secretion in cholera. *Gastroenterology* **132:**1234–1244.
Tikhonov DB and Magazanik LG (1998) Voltage dependence of open channel blockade: onset and offset rates. *J Membr Biol* **161:**1–8.
Villoutreix BO, Eudes R, and Miteva MA (2009) Structure-based virtual ligand screening: recent success stories. *Comb Chem High Throughput Screen* **12:**1000–1016.
Wang J, Wang W, Kollman PA, and Case DA (2006) Automatic atom type and bond type perception in molecular mechanical calculations. *J Mol Graph Model* **25:**247–260.
Wang W and Linsdell P (2012) Alternating access to the transmembrane domain of the ATP-binding cassette protein cystic fibrosis transmembrane conductance regulator (ABCC7). *J Biol Chem* **287:**10156–10165.
Ward A, Reyes CL, Yu J, Roth CB, and Chang G (2007) Flexibility in the ABC transporter MsbA: alternating access with a twist. *Proc Natl Acad Sci USA* **104:**19005–19010.
Woodhull AM (1973) Ionic blockage of sodium channels in nerve. *J Gen Physiol* **61:**687–708.
Yang B, Sonawane ND, Zhao D, Somlo S, and Verkman AS (2008) Small-molecule CFTR inhibitors slow cyst growth in polycystic kidney disease. *J Am Soc Nephrol* **19:**1300–1310.
Zhang ZR, Cui G, Zeltwanger S, and McCarty NA (2004a) Time-dependent interactions of glibenclamide with CFTR: kinetically complex block of macroscopic currents. *J Membr Biol* **201:**139–155.
Zhang ZR, Song B, and McCarty NA (2005) State-dependent chemical reactivity of an engineered cysteine reveals conformational changes in the outer vestibule of the cystic fibrosis transmembrane conductance regulator. *J Biol Chem* **280:**41997–42003.
Zhang ZR, Zeltwanger S, and McCarty NA (2004b) Steady-state interactions of glibenclamide with CFTR: evidence for multiple sites in the pore. *J Membr Biol* **199:**15–28.
Zhou JJ, Fatehi M, and Linsdell P (2007) Direct and indirect effects of mutations at the outer mouth of the cystic fibrosis transmembrane conductance regulator chloride channel pore. *J Membr Biol* **216:**129–142.
Zhou JJ, Li MS, Qi J, and Linsdell P (2010) Regulation of conductance by the number of fixed positive charges in the intracellular vestibule of the CFTR chloride channel pore. *J Gen Physiol* **135:**229–245.
Zhou Z, Hu S, and Hwang TC (2002) Probing an open CFTR pore with organic anion blockers. *J Gen Physiol* **120:**647–662.

Address correspondence to: Dr. Yohei Norimatsu, Department of Physiology and Pharmacology, Oregon Health and Science University, 3181 SW Sam Jackson Park Rd., Portland, OR 97239. E-mail: norimats@ohsu.edu